IEEE Access
Multidisciplinary ⋮ Rapid Review ⋮ Open Access Journal

Received May 5, 2021, accepted May 16, 2021, date of publication May 19, 2021, date of current version June 2, 2021.

Digital Object Identifier 10.1109/ACCESS.2021.3081986

Efficient Enhanced Hybrid Implicit-Explicit Procedure to Gyrotropic Plasma in Open Regions With Fine Geometry Details Along Single Direction

PEIYU WU[1], (Graduate Student Member, IEEE), HAN YU[2], YONGJUN XIE[1], HAOLIN JIANG[3], (Member, IEEE), AND TOSHIAKI NATSUKI[4,5]

[1]School of Electronic and Information Engineering, Beihang University, Beijing 100191, China
[2]Beijing Institute of Astronautical Systems Engineering, Beijing 100076, China
[3]School of Information Science and Engineering, Southeast University, Southeast University, Nanjing 210096, China
[4]Faculty of Textile Science and Technology, Shinshu University, Ueda 386-8567, Japan
[5]Institute of Carbon Science and Technology, Shinshu University, Nagano 380-8553, Japan

Corresponding authors: Yongjun Xie (yjxie@buaa.edu.cn), Haolin Jiang (haolinjiang.cem@gmail.com), and Toshiaki Natsuki (natsuki@shinshu-u.ac.jp)

This work was supported in part by the National Natural Science Foundation of China under Grant 61571022, Grant 61971022, and Grant 61801376; and in part by the National Key Laboratory Foundation of China under Grant HTKJ2019KL504013 and Grant 61424020305.

ABSTRACT For the simulation of gyrotropic plasma structure with fine geometry details along a single direction in open regions, the hybrid implicit-explicit (HIE) algorithm with improved absorbing boundary condition is modified based on the finite-difference time-domain (FDTD) algorithm. More precisely, incorporating the perfectly matched layer (PML) formulation, the higher order concept and the HIE procedure, the proposed implementation shows its significant superiority in terms of efficiency, accuracy and absorption. To simulate the unique anisotropic characteristic inside the gyrotropic plasma regions, the bilinear transform (BT) method is employed during the calculation. The effectiveness can be further demonstrated theoretically and numerically. Through the results, it can be concluded that the proposed scheme exhibits remarkable behaviors in the gyrotropic plasma open region problems. It can not only obtain considerable accuracy compared with the theoretical solution but also receive better absorption and efficiency compared with the published work. In addition, the results also indicate that the proposed scheme can maintain the stability of the algorithm with dissatisfaction of the Courant-Friedrichs-Levy condition between time step and mesh size.

INDEX TERMS Anisotropic gyrotropic plasma, bilinear transform (BT), finite-difference time-domain (FDTD), hybrid implicit-explicit (HIE), perfectly matched layer (PML).

I. INTRODUCTION

With significant advantages in broadband simulation, the finite-difference time-domain (FDTD) algorithm has become one of the most widely spread numerical simulation methods. Especially with the time-varying dispersion medium, the FDTD algorithm can obtain the electromagnetic properties within a single run [1]–[3]. While the frequency domain based algorithms must calculate the results in the separate frequency, the FDTD algorithm can obtain better efficiency during the entire calculation [4]. However, such implementation becomes inaccurate in the simulation of fine structures or large number of time steps problems. Because of the existence of the CFL condition, the relationship is established between the mesh size and time step [5]. By applying the FDTD algorithm directly to them, extensive duration leads to the unacceptable calculation. To maintain considerable calculation accuracy and enhance the efficiency at the same time, many methods are introduced to achieve such objective. One of the most efficient ways is the employment of unconditionally stable algorithms including alternating direction implicit (ADI), locally one-dimensional (LOD),

The associate editor coordinating the review of this manuscript and approving it for publication was Muhammad Zubair.

Crank-Nicolson (CN) procedures [6]–[8]. Although they can overcome the CFL condition, the numerical dispersion increases significantly with the enlargement of CFL numbers (CFLNs) [9]. Such phenomenon becomes much more significant especially in the structures with fine geometry details along a single direction. In such circumstance, extremely fine mesh size results in the decrement of accuracy and efficiency. Fortunately, hybrid implicit-explicit (HIE) procedure is proposed to alleviate such condition [10], [11]. Compared with the other unconditionally stable algorithms, the HIE procedure merely solves two tri-diagonal matrices within a single iteration which significantly reduces the calculation complexity [12]–[14]. Meanwhile, it can receive lower numerical dispersion with property CFLNs [15], [16].

In open region problems, it has been demonstrated that the absorbing boundary condition must be employed for the termination of unbounded domains [4], [5]. The perfectly matched layer (PML) is one of the most popular methods for the simulation of domain extension [17]. The original PML with six auxiliary variables which is implemented by split-field scheme shows its disadvantages in accuracy, efficiency and absorption [18]. To overcome these disadvantages, the stretched coordinate (SC) PML is developed to simplify the implementation at corners and edges [19]. Although SC-PML can improve the entire performance compared with the original split-field PML, it has been testified that the performance at low-frequency and in late-time still need to be improved during the whole simulation [18]. The complex-frequency-shifted (CFS) PML is proposed to alleviate such conditions by attenuating low-frequency evanescent waves and reducing late-time reflections [20]. In some problems with large amount of low-frequency waves, CFS-PML shows feeble performance especially in the frequency domain. The reason is that the reflection of low-frequency propagation waves still maintains a higher level. The higher order concept is incorporated with PML formulation not only to solve such problem but also to further enhance the absorption [21]. The most prominent disadvantage is the significant increment of auxiliary variables and coefficients resulting in decrement of efficiency [22]–[24]. Thus, unconditionally stable algorithms are introduced into the higher order PML implementations [25]–[29].

The numerical simulation of dispersion materials has become a frontier science. The dispersion material includes isotropic and anisotropic materials [30]. Among them, the anisotropic materials including electric anisotropic materials and magnetic anisotropic materials have gained considerable attention due to its unique anisotropic behavior. However, such special materials cannot be obtained from nature directly. Thus, the simulation on anisotropic materials is becoming increasingly important, especially for the aerospace industry, plasma sheath on the surface of flight vehicle and wave transmission inside the plasma regions [31]–[33]. Basically, the simulations of interactions between the plasma and electromagnetic wave are performed by using the particle-in-cell method, which is based on the finite difference time domain (FDTD) method, or the FDTD method combined with the effective permittivity model [34], [35]. For the FDTD method, several methods have been developed including the recursive convolution method, auxiliary differential equation method, Z transform method, current density convolution method [36]–[39]. Among these typical methods, the z transform by bilinear method, usually called bilinear transform (BT), the most considerable entire efficiency and accuracy [40].

Until now, several higher order PML algorithms have been developed into the anisotropic gyrotropic plasma simulation [41], [42]. It should be noticed that they can merely solve the Maxwell's equations in two-dimensions. Recently, the ADI and CN procedures are combined with the gyrotropic plasma simulation for the three-dimensions [43], [44]. Although all of them can overcome the CFL condition, the limitations with fine geometry details along single direction structures still need to be perfected.

Here, by incorporating the higher order concept, HIE procedure and PML formulation, an alternative implementation is proposed for the gyrotropic plasma structures which have fine geometry details along a single direction in open regions. The unique anisotropic property of gyrotropic plasma can be simulated and calculated by the BT method. The effectiveness can be demonstrated theoretically and numerically. From the results, it can be concluded that the proposed scheme holds considerable entire performance.

II. FORMULATIONS

For the simulation of anisotropic gyrotropic plasma, the Maxwell's equations inside the higher order PML (HPML) regions can be expressed as

$$j\omega\mathbf{D} = \nabla_s \times \mathbf{H} \tag{1a}$$

$$j\omega\mu_0\mathbf{H} = -\nabla_s \times \mathbf{E} \tag{1b}$$

where the electric displacement vector $\mathbf{D} = \varepsilon_0\varepsilon_r\mathbf{E}$ can be expressed as

$$\mathbf{D} = \mathbf{E} + \mathbf{J} \tag{1c}$$

where $\mathbf{E}$ is the electric component and J is the polarization current density which can be given as

$$j\omega\mathbf{J} = \varepsilon_0\omega_p^2\mathbf{E} - \nu\mathbf{J} + \omega_b\mathbf{J} \tag{1d}$$

where ν is the damping constant, ω_p is the plasma frequency and ω_b is the electron gyro-frequency representing the direction of magnetization [45]. Within (1a)-(1b), the operator can be given as

$$\nabla_s = \hat{x}\frac{1}{S_x}\frac{\partial}{\partial x} + \hat{y}\frac{1}{S_y}\frac{\partial}{\partial y} + \hat{z}\frac{1}{S_z}\frac{\partial}{\partial z} \tag{1e}$$

where the stretched coordinate variables with higher order concept along different directions is

$$S_\eta = \left(\kappa_{\eta 1} + \frac{\sigma_{\eta 1}}{\alpha_{\eta 1} + j\omega\varepsilon_0}\right)\left(\kappa_{\eta 2} + \frac{\sigma_{\eta 2}}{\alpha_{\eta 2} + j\omega\varepsilon_0}\right) \tag{1f}$$

where $\kappa_{\eta n} \geq 1, \eta = x, y, z, n = 1, 2$ is assumed to be bigger than 1, $\sigma_{\eta n}$ and $\alpha_{\eta n}$ are assumed to be larger than 0. According to the bilinear transform by firstly transforming S_η^{-1} into s-domain according to $j\omega \leftrightarrow s$, and then employing the BT method according to the relationship $s \leftrightarrow (2/\Delta t)\left[\left(1-z^{-1}\right)/\left(1+z^{-1}\right)\right]$. Equation (1f) can be given in the z-domain as

$$S_\eta(z) = w_{\eta 1} w_{\eta 2} \frac{1 - a_{\eta 1} z^{-1}}{1 - b_{\eta 1} z^{-1}} \frac{1 - a_{\eta 2} z^{-1}}{1 - b_{\eta 2} z^{-1}} \tag{2}$$

where the coefficients can be given as

$$w_{\eta n} = \frac{1}{\kappa_{\eta n}}\{(\frac{2}{\Delta t} + \frac{\alpha_{\eta n}}{\varepsilon_0})/[\frac{2}{\Delta t} + (\frac{\alpha_{\eta n}}{\varepsilon_0} + \frac{\sigma_{\eta n}}{\kappa_{\eta n}\varepsilon_0})]\},$$
$$a_{\eta n} = [(\frac{2}{\Delta t} - \frac{\alpha_{\eta n}}{\varepsilon_0})/(\frac{2}{\Delta t} + \frac{\alpha_{\eta n}}{\varepsilon_0})]$$

and

$$b_{\eta n} = \{[\frac{2}{\Delta t} - (\frac{\alpha_{\eta n}}{\varepsilon_0} + \frac{\sigma_\eta}{\kappa_\eta \varepsilon_0})]/[\frac{2}{\Delta t} + (\frac{\alpha_\eta}{\varepsilon_0} + \frac{\sigma_\eta}{\kappa_\eta \varepsilon_0})]\}.$$

By substituting (1c) into (1a), the Maxwell's equations can be given as

$$\varepsilon_0 \frac{1 - z^{-1}}{\Delta t}\mathbf{E} = (\mathbf{A} - \mathbf{B})\,\mathbf{H} - \mathbf{J} \tag{3a}$$
$$\mu_0 \frac{1 - z^{-1}}{\Delta t}\mathbf{H} = (\mathbf{B} - \mathbf{A})\,\mathbf{E} \tag{3b}$$

where $E = \left[E_x, E_y, E_z\right]^T$, $H = \left[H_x, H_y, H_z\right]^T$, $J = \left[J_x, J_y, J_z\right]^T$,

$$\mathbf{A} = \begin{bmatrix} 0 & 0 & S_y(z)\,\partial_y \\ S_z(z)\,\partial_z & 0 & 0 \\ 0 & S_x(z)\,\partial_x & 0 \end{bmatrix}$$

and

$$\mathbf{B} = \begin{bmatrix} 0 & S_z(z)\,\partial_z & 0 \\ 0 & 0 & S_x(z)\,\partial_x \\ S_y(z)\,\partial_y & 0 & 0 \end{bmatrix}.$$

Supposing the magnetic direction along z-direction, the relative permittivity inside the anisotropic gyrotropic plasma can be expressed as

$$\varepsilon_r = \begin{bmatrix} \varepsilon_{xx} & -\varepsilon_{xy} & 0 \\ -\varepsilon_{yx} & \varepsilon_{yy} & 0 \\ 0 & 0 & \varepsilon_{zz} \end{bmatrix} \tag{3c}$$

where $\varepsilon_{xx} = \varepsilon_{yy} = \varepsilon_{zz} = \omega_p^2$, $\varepsilon_{xy} = \varepsilon_{yx} = -\nu + \omega_b$. By applying the z-transformation to (1c), one obtains

$$\frac{1 - z^{-1}}{\Delta t}\mathbf{J} = \varepsilon_0 \omega_p^2 \mathbf{E} - \nu \mathbf{J} + \omega_b \mathbf{J} \tag{3d}$$

By substituting (2) into (3a)-(3b) and introducing the auxiliary variables, the equations and (3d)can be further manipulated as

$$\mathbf{E} = z^{-1}\mathbf{E} + \mathbf{C}_e\mathbf{F} + (A_e - \mathbf{B}_e)\,\mathbf{H} - \frac{\Delta t}{\varepsilon_0}\mathbf{J} \tag{4a}$$
$$\mathbf{H} = z^{-1}\mathbf{H} + (\mathbf{B}_h - \mathbf{A}_h)\,\mathbf{E} \tag{4b}$$
$$\mathbf{J} = z^{-1}\mathbf{J} + \Delta t \varepsilon_0 \omega_p^2 \mathbf{E} - \nu \Delta t \mathbf{J} + \omega_b \Delta t \mathbf{J} \tag{4c}$$

where the matrix are given as $\mathbf{F} = \left[F_{x\eta n}; F_{y\eta n}; F_{z\eta n}\right]$, $\mathbf{F} = \left[F_{xy1}, F_{xy2}, F_{xz1}, F_{xz2}\right]$,

$$\mathbf{C}_\zeta = \begin{bmatrix} p_{1\zeta y} & p_{2\zeta y} & p_{1\zeta z} & p_{2\zeta z} \\ p_{1\zeta z} & p_{1\zeta x} & p_{1\zeta z} & p_{2\zeta z} \\ p_{1\zeta x} & p_{1\zeta x} & p_{1\zeta y} & p_{2\zeta y} \end{bmatrix}, \quad \zeta = e, h,$$
$$\mathbf{A}_\zeta = \begin{bmatrix} 0 & -p_{3\zeta z}\delta_z & p_{3\zeta y}\delta_y \\ p_{3\zeta z}\delta_z & 0 & 0 \\ 0 & 0 & 0 \end{bmatrix},$$
$$\mathbf{B}_\zeta = \begin{bmatrix} 0 & 0 & 0 \\ 0 & 0 & p_{3\zeta x}\delta_x \\ p_{3\zeta y}\delta_y & -p_{3\zeta x}\delta_x & 0 \end{bmatrix},$$

the operator δ_η is the finite-difference form, the other coefficients according to the HIE procedure are $p_{1e\eta} = \Delta t\left(a_{\eta 2} - b_{\eta 1}\right)/(2\varepsilon_0)$, $p_{2e\eta} = \Delta t\left(a_{\eta 1} - b_{\eta 2}\right)/(2\varepsilon_0)$, $p_{3e\eta} = \Delta t k_\eta/(2\varepsilon_0)$, $p_{1h\eta} = \Delta t\left(a_{\eta 2} - b_{\eta 1}\right)/(2\mu_0)$, $p_{2h\eta} = \Delta t\left(a_{\eta 1} - b_{\eta 2}\right)/(2\mu_0)$, $p_{3h\eta} = \Delta t k_\eta/(2\mu_0)$. According to the standard HIE procedure and supposing the fine grids distributes along z-direction, the equations can be given as

$$\begin{aligned} E_z^{n+1/2} = {} & E_z^{n-1/2} + p_{1ex}F_{zx2}^{n-1/2} + p_{2ex}F_{zx1}^{n-1/2} \\ & + p_{3ex}\delta_x H_y^n - p_{1ey} \\ & \times F_{zy2}^{n-1/2} - p_{2ey}F_{zy1}^{n-1/2} - p_{3ey}\delta_y H_x^n \\ & - p_{4ey}\left(J_z^{n+1/2} + J_z^{n-1/2}\right) \end{aligned} \tag{5a}$$

$$\begin{aligned} H_z^{n+1/2} = {} & H_z^{n-1/2} + p_{1hy}G_{zy2}^{n-1/2} + p_{2hy}G_{zy1}^{n-1/2} \\ & + p_{3hy}\delta_y E_x^n \\ & - p_{1hx}G_{zx2}^{n-1/2} - p_{2hx}G_{zx1}^{n-1/2} - p_{3hx}\delta_x E_y^n \end{aligned} \tag{5b}$$

The other field components can be given as

$$\begin{aligned} E_x^{n+1} = {} & E_x^n - p_{1ez}F_{xz2}^n - p_{2ez}F_{xz1}^n - p_{3ez}\delta_z\left(H_y^{n+1} + H_y^n\right) \\ & + p_{1ey}F_{xy2}^n + p_{2ey}F_{xy1}^n + p_{3ey}\delta_y H_z^{n+1/2} \\ & - p_{4ex}\left(J_x^{n+1} + J_x^n\right) \end{aligned} \tag{6a}$$

$$\begin{aligned} E_y^{n+1} = {} & E_y^n + p_{1ez}F_{yz2}^n + p_{2ez}F_{yz1}^n + p_{3ez}\delta_z\left(H_x^{n+1} + H_x^n\right) \\ & - p_{1ex}F_{yx2}^n - p_{2ex}F_{yx1}^n - p_{3ex}\delta_x H_z^{n+1/2} \\ & - p_{4ey}\left(J_y^{n+1} + J_y^n\right) \end{aligned} \tag{6b}$$

$$\begin{aligned} H_x^{n+1} = {} & H_x^n + p_{1hz}G_{xz2}^n + p_{2hz}G_{xz1}^n + p_{3hz}\delta_z\left(E_y^{n+1} + E_y^n\right) \\ & - p_{1hy}G_{xy2}^n - p_{2hy}G_{xy1}^n - p_{3hy}\delta_y E_z^{n+1/2} \end{aligned} \tag{6c}$$

$$\begin{aligned} H_y^{n+1} = {} & H_y^n - p_{1hz}G_{yz2}^n - p_{2hz}G_{yz1}^n - p_{3hz}\delta_z\left(E_x^{n+1} + E_x^n\right) \\ & + p_{1hx}G_{yx2}^n + p_{2hx}G_{yx1}^n + p_{3hx}\delta_x E_z^{n+1/2} \end{aligned} \tag{6d}$$

It can be observed that the calculation of (5a)-(6d) can be divided into two parts including:

1) Calculation of the HIE-FDTD procedure
2) Wave propagation in the anisotropic gyrotropic plasma

A. CALCULATION OF THE HIE-FDTD PROCEDURE

By substituting (6d) into (6a) to eliminate H_y^{n+1}, the results can be given as

$$\begin{aligned}(1-p_{3hz}p_{3ez}\delta_z\delta_z)\,E_x^{n+1}&=(1+p_{3hz}p_{3ez}\delta_z\delta_z)\,E_x^n\\&-p_{1ez}F_{xz2}^n-p_{2ez}F_{xz1}^n+p_{1ey}F_{xy2}^n+p_{2ey}F_{xy1}^n\\&+p_{1hz}p_{3ez}\delta_z G_{yz2}^n+p_{2hz}p_{3ez}\delta_z G_{yz1}^n-p_{1hx}p_{3ez}\delta_z G_{yx2}^n\\&-p_{2hx}p_{3ez}\delta_z G_{yx1}^n-2p_{3ez}\delta_z H_y^n+p_{3ey}\delta_y H_z^{n+1/2}\\&-p_{3hx}p_{3ez}\delta_z\delta_x E_z^{n+1/2}-p_{4ex}\left(J_x^{n+1}+J_x^n\right)\end{aligned}\tag{7}$$

By substituting (6c) into (6b) to eliminate H_x^{n+1}, one obtains

$$\begin{aligned}(1-p_{3hz}p_{3ez}\delta_z\delta_z)\,E_y^{n+1}&=(1+p_{3hz}p_{3ez}\delta_z\delta_z)\,E_y^n\\&+p_{1ez}F_{yz2}^n+p_{2ez}F_{yz1}^n-p_{1ex}F_{yx2}^n-p_{2ex}F_{yx1}^n\\&+p_{1hz}p_{3ez}\delta_z G_{xz2}^n+p_{2hz}p_{3ez}\delta_z G_{xz1}^n-p_{1hy}p_{3ez}\delta_z G_{xy2}^n\\&-p_{2hy}p_{3ez}\delta_z G_{xy1}^n-p_{3hy}p_{3ez}\delta_z\delta_y E_z^{n+1/2}+2p_{3ez}\delta_z H_x^n\\&-p_{3ex}\delta_x H_z^{n+1/2}-p_{4ey}\left(J_y^{n+1}+J_y^n\right)\end{aligned}\tag{8}$$

It can be observed that two tridiagonal matrices are formed by $(1-p_{3hz}p_{3ez}\delta_z\delta_z)\,E_x^{n+1}$ and $(1-p_{3hz}p_{3ez}\delta_z\delta_z)\,E_y^{n+1}$. They can be solved by the Thomas algorithm. However, it can also be observed that the polarization current density and the electric field density are coupled which results in the updating unable to realize. The simulation should introduce the method to solve the wave propagation in the anisotropic gyrotropic plasma.

B. WAVE PROPAGATION IN THE ANISOTROPIC GYROTROPIC PLASMA

The polarization current density in different directions can be given in the z-domain as

$$\frac{1-z^{-1}}{\Delta t}J_x+\nu J_x=\varepsilon_0\omega_p^2E_x-\omega_bJ_y\tag{9a}$$

$$\frac{1-z^{-1}}{\Delta t}J_y+\nu J_y=\varepsilon_0\omega_p^2E_y+\omega_bJ_x\tag{9b}$$

$$\frac{1-z^{-1}}{\Delta t}J_z=\varepsilon_0\omega_p^2E_z\tag{9c}$$

It can be observed from (9a) and (9b) that J_x and J_y are coupled due to its unique anisotropic characteristic. Thus, the two components should be updated at the same time to maintain the stability of the algorithm. By substituting (9b) into (9a) and (9a) into (9b), the equations can be given in the FDTD domain as

$$\begin{aligned}J_x^{n+1}&=p_{1j}J_x^n-p_{2j}J_y^n+p_{3j}E_x^{n+1}+p_{3j}E_x^n\\&\quad-p_{4j}E_y^{n+1}-p_{4j}E_y^n\end{aligned}\tag{10a}$$

$$\begin{aligned}J_y^{n+1}&=p_{1j}J_y^n+p_{2j}J_x^n+p_{3j}E_y^{n+1}+p_{3j}E_y^n\\&\quad+p_{4j}E_x^{n+1}+p_{4j}E_x^n\end{aligned}\tag{10b}$$

$$J_z^{n+1/2}=J_z^{n-1/2}+p_{5j}E_z^{n-1/2}\tag{10c}$$

where $p_{1j}=[1-(\nu\Delta t/4)^2-(\omega_b\Delta t/4)^2]/p_{6j}$, $p_{2j}=\omega_b\Delta t/p_{6j}$, $p_{3j}=[\varepsilon_0\Delta t\omega_p^2(1+\nu\Delta t/4)]/p_{6j}$, $p_{4j}=(\varepsilon_0\Delta t^2\omega_p^2\omega_b)/(2p_{6j})$, $p_{5j}=(1+\nu\Delta t/4)^2+(\omega_b\Delta t/4)^2$ and $p_{6j}=\varepsilon_0\omega_p^2\Delta t/4$.

C. JOINT SOLUTION COMBINED HIE PROCEDURE AND ANISOTROPIC GYROTROPIC PLASMA SIMULATION

The final updated equation can be obtained by incorporating the HIE procedure and calculation of anisotropic gyrotropic plasma. By substituting (10a)-(10c) to (5a), (7) and (8), respectively, the equations can be obtained as

$$\begin{aligned}\left(1-p_{3hz}p_{3ez}\delta_z\delta_z+p_{4ex}p_{3j}\right)E_x^{n+1}&=\left(1+p_{3hz}p_{3ez}\delta_z\delta_z-p_{4ex}p_{3j}\right)E_x^n\\&-p_{1ez}F_{xz2}^n-p_{2ez}F_{xz1}^n+p_{1ey}F_{xy2}^n+p_{2ey}F_{xy1}^n\\&+p_{1hz}p_{3ez}\delta_z G_{yz2}^n+p_{2hz}p_{3ez}\delta_z G_{yz1}^n\\&-p_{1hx}p_{3ez}\delta_z G_{yx2}^n-p_{2hx}p_{3ez}\delta_z G_{yx1}^n-2p_{3ez}\delta_z H_y^n\\&+p_{3ey}\delta_y H_z^{n+1/2}-p_{3hx}p_{3ez}\delta_z\delta_x E_z^{n+1/2}\\&-p_{4ex}\left(1+p_{1j}\right)J_x^n+p_{4ex}p_{2j}J_y^n\\&+p_{4ex}p_{4j}E_y^{n+1}+p_{4ex}p_{4j}E_y^n\end{aligned}\tag{11}$$

$$\begin{aligned}\left(1-p_{3hz}p_{3ez}\delta_z\delta_z+p_{4ey}p_{4j}\right)E_y^{n+1}&=\left(1+p_{3hz}p_{3ez}\delta_z\delta_z-p_{4ey}p_{4j}\right)E_y^n+p_{1ez}F_{yz2}^n\\&+p_{2ez}F_{yz1}^n-p_{1ex}F_{yx2}^n-p_{2ex}F_{yx1}^n\\&+p_{1hz}p_{3ez}\delta_z G_{xz2}^n+p_{2hz}p_{3ez}\delta_z G_{xz1}^n\\&-p_{1hy}p_{3ez}\delta_z G_{xy2}^n-p_{2hy}p_{3ez}\delta_z G_{xy1}^n\\&-p_{3hy}p_{3ez}\delta_z\delta_y E_z^{n+1/2}+2p_{3ez}\delta_z H_x^n\\&-p_{3ex}\delta_x H_z^{n+1/2}-p_{4ey}\left(1+p_{1j}\right)J_y^n\\&-p_{4ey}p_{2j}J_x^n-p_{4ey}p_{3j}E_y^{n+1}-p_{4ey}p_{3j}E_y^n\end{aligned}\tag{12}$$

$$\begin{aligned}E_z^{n+1/2}&=\left(1-p_{4ey}p_{5j}\right)E_z^{n-1/2}\\&+p_{1ex}F_{zx2}^{n-1/2}+p_{2ex}F_{zx1}^{n-1/2}+p_{3ex}\delta_x H_y^n\\&-p_{1ey}F_{zy2}^{n-1/2}-p_{2ey}F_{zy1}^{n-1/2}\\&-p_{3ey}\delta_y H_x^n-2p_{4ey}J_z^{n-1/2}\end{aligned}\tag{13}$$

According to (11)-(13), the electric field can be innovated by two implicit and one explicit equations. Once the electric component is calculated out, the other components, polarization current density and auxiliary variables can be solved at the same time. The entire updated cycle can be described as follows:

1) Save the components among the calculation previous time step.
2) Explicitly update E_z and H_z according to (13) and (5b).
3) Implicitly update E_x and E_y according to (11) and (12).
4) Explicitly update H_x and H_y according to (6c) and (6d).
5) Explicitly update polarization current density and auxiliary variables.

The corresponding flow chart of the entire calculation is shown in Fig. 1. Through the flow chart, all of the component can be updated.

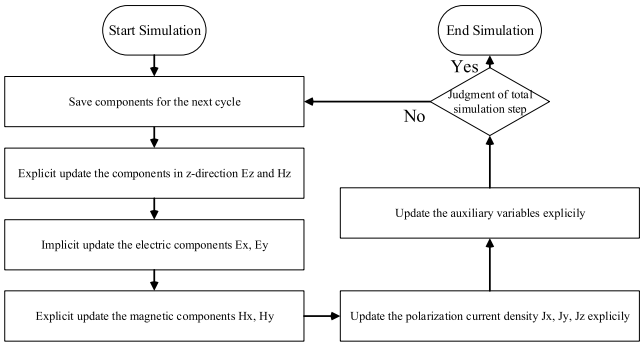

FIGURE 1. The flow chart of the entire calculation within the proposed HIE-HPML procedure.

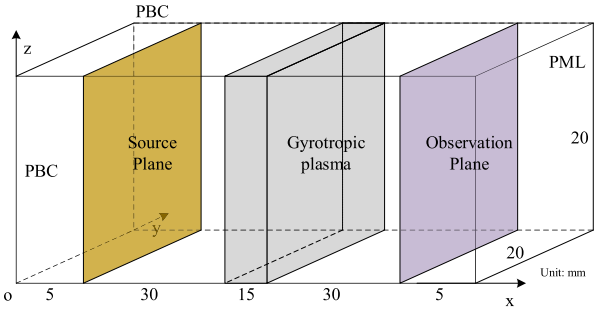

FIGURE 2. The sketch picture of anisotropic gyrotropic plasma slab model.

Until now, several methods have been developed for the investigation of anisotropic gyrotropic plasma including the weighted laguerre polynomials, ADI, LOD, CN procedures [41]–[44], [46], [47]. All of these procedures belong to the unconditionally stable algorithms which shows significant decrement of efficiency and accuracy when simulating the fine geometry details along a single direction. Although the conventional FDTD algorithm shows considerable calculation accuracy, the efficiency remains unacceptable. For making comparisons between the proposed procedure and previous work and demonstrating the effectiveness of the proposed implementation, several procedures are selected including the FDTD-PML in [48], ADI-HPML in [29], CNDS-HPML in [49], CNAFS-HPML in [49]. The FDTD-HPML is also implementation based on the conventional FDTD algorithm.

III. NUMERICAL RESULTS AND DISCUSSION

Numerical examples are carried out to demonstrate the effectiveness and efficiency both theoretically and numerically. Three examples which correspond to different kinds of problems are carried out including the wave reflection/transmission and wave propagation problems.

A. WAVE REFLECTION AND TRANSMISSION PROBLEM: AN ANISOTROPIC GYROTROPIC PLASMA SLAB MODEL

The wave transmission and reflection through the anisotropic gyrotropic plasma slab is considered. Such problem has its analytic resolution. The accuracy can be reflected through the comparison between the test solution and analytic resolution. The anisotropic gyrotropic plasma slab holds the parameters of $\omega_p = 2\pi \times 28.7$ GHz, $\omega_b = 0.1$ Trad/s and $\nu = 20$ Grad/s [45]. The entire computational domain is shown as Fig. 2. The fine geometry details are existed along the x-direction. The y- and z-directions hold rough mesh.

The anisotropic gyrotropic plasma slab with 15 mm along x-direction is located at the middle. The whole computational domain holds the directions of $85 \times 20 \times 20$ mm. The source is a modulated Gaussian pulse with the bandwidth and center frequency of 50 GHz propagates along the positive x-direction. The position between the left boundary and the slab of x-direction are 5 mm and 30 mm, respectively. At the right side of the domain, the observation plane is located at 30 mm and 5 mm between the slab and right boundary. The boundaries of x-direction are terminated by 10-cell-PML to ensure the calculation accuracy. The y- and z-directions are terminated by the perfectly boundary condition (PBC). In the HPML regions, the parameters are chosen by try and error method to obtain the best absorption which reduces the influence between reflection waves and transmission waves. The parameters can be chosen as follows: $\kappa_{\eta 1} = 240$, $\alpha_{\eta 1} = 0.2$, $m_{\eta 1} = 3$, $\sigma_{\eta 1\_\max} = 1.3\sigma_{\eta 1\_opt}$, $\kappa_{\eta 2} = 2$, $\alpha_{\eta 2}$=0.8, $m_{\eta 2} = 1$, $\sigma_{\eta 2\_\max} = 0.01\sigma_{\eta 2\_opt}$, where

$$\sigma_{\eta n\_opt} = (m_{\eta n} + 1)/(150\pi\Delta\eta) \tag{14}$$

For the CFS-PML based algorithms, the corresponding parameters are employed as $\kappa_\eta = 200$, $\alpha_\eta = 2.4$, $m_\eta = 3$, $\sigma_{\eta\_\max} = 1.7\sigma_{\eta\_opt}$. To simulate the fine details along single direction and compare performance between different algorithms, the mesh size can be chosen as $\Delta x = 30\mu$m and $\Delta y = \Delta z = 0.15$ mm. It can also be observed from Fig. 2 that fine details are distributed along x-direction. The time step employed in the conventional FDTD algorithm can be calculated as $\Delta t_{\max}^{FDTD} = 57.7$ fs which satisfies the CFL condition. The CFL number (CFLN) can be defined as $CFLN = \Delta t \big/ \Delta t_{\max}^{FDTD}$. Within the equation, Δt is the time step in the algorithms whose stability can break the CFL condition. The accuracy can be obtained by the transmission and reflection coefficients of right circularly polarized (RCP) and left circularly polarized (LCP). Figure 3 indicates the transmission coefficient of RCP obtained by different PML algorithms and CFLNs. Meanwhile, Figure 4 also demonstrates the transmission coefficient of LCP obtained by them.

As shown in Fig. 3 (a) and Fig. 4(a) that curves obtained by the different PML algorithms are overlapped indicating that they almost hold the same accuracy with CFLN = 1. From the other figures, it can be concluded that the accuracy decreases with the increment of CFLNs. The reason is the numerical dispersion increases with the enlargement of CFLNs. Furthermore, it can be concluded that the ADI-HPML is with the worst performance among the PML algorithms whose stability are not limited by the CFL condition.

In addition, it can be concluded the CNAFS and HIE procedure have the best performance. Compared with the FDTD-PML, it can be observed that the FDTD-HPML has

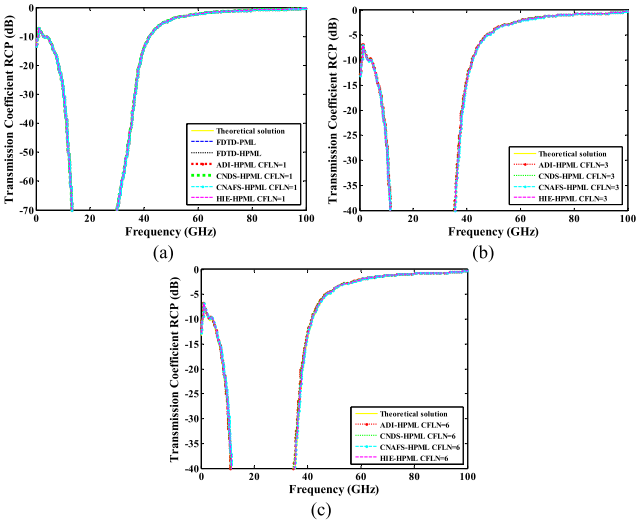

FIGURE 3. The transmission coefficient of RCP wave (a) FDTD-PML, FDTD-HPML, ADI-HPML, CNDS-HPML, CNAFS-HPML and HIE-HPML CFLN = 1. (b) ADI-HPML, CNDS-HPML, CNAFS-HPML and HIE-HPML CFLN = 3. (c) ADI-HPML, CNDS-HPML, CNAFS-HPML and HIE-HPML CFLN = 6.

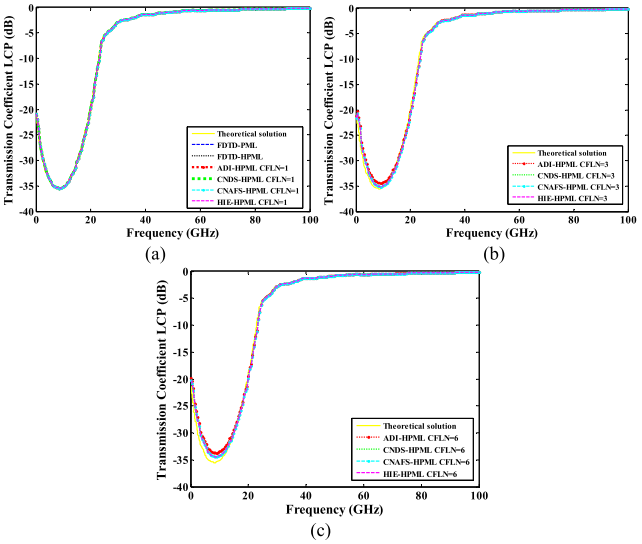

FIGURE 4. The transmission coefficient of LCP wave (a) FDTD-PML, FDTD-HPML, ADI-HPML, CNDS-HPML, CNAFS-HPML and HIE-HPML CFLN = 1. (b) ADI-HPML, CNDS-HPML, CNAFS-HPML and HIE-HPML CFLN = 3. (c) ADI-HPML, CNDS-HPML, CNAFS-HPML and HIE-HPML CFLN = 6.

better accuracy during the calculation. Such phenomenon indicates the higher order formulation can improve the accuracy of the calculation. Figure 5 and Fig. 6 demonstrate the LCP and RCS reflection coefficients of the anisotropic gyrotropic plasma slab, respectively.

It can be obtained the same conclusions as previous that the different PML algorithms hold the same accuracy with lower CFLNs and become worse with the increment of CFLNs. However, it can be observed that the performance of different PML algorithms cannot be distinguished sometimes. To compare the accuracy of different PML algorithms, the root mean square (RMS) error is introduced during the simulation. The theoretical solution is chosen as the basis for comparison.

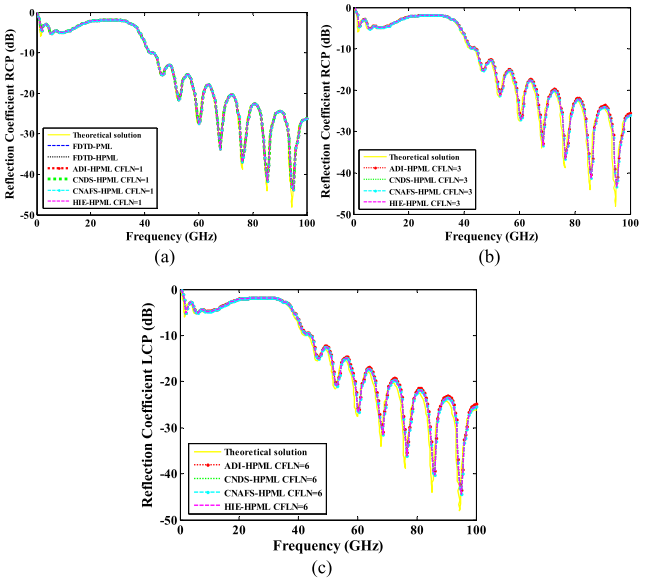

FIGURE 5. The reflection coefficient of RCP wave (a) FDTD-PML, FDTD-HPML, ADI-HPML, CNDS-HPML, CNAFS-HPML and HIE-HPML CFLN = 1. (b) ADI-HPML, CNDS-HPML, CNAFS-HPML and HIE-HPML CFLN = 3. (c) ADI-HPML, CNDS-HPML, CNAFS-HPML and HIE-HPML CFLN = 6.

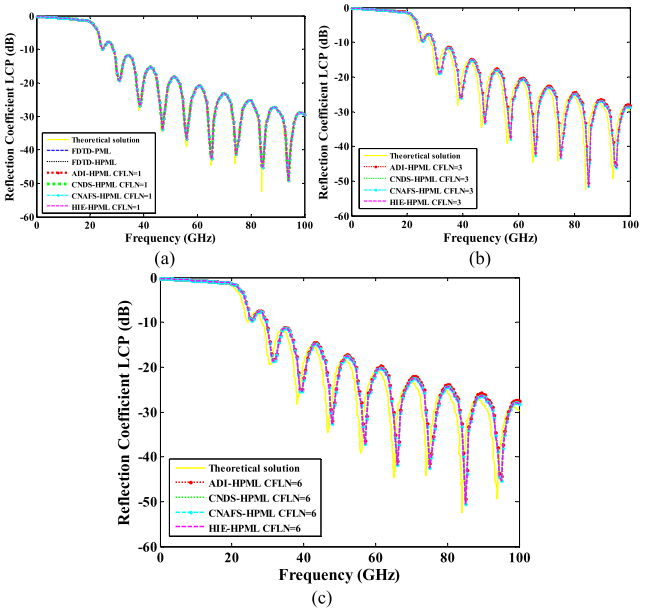

FIGURE 6. The reflection coefficient of LCP wave (a) FDTD-PML, FDTD-HPML, ADI-HPML, CNDS-HPML, CNAFS-HPML and HIE-HPML CFLN = 1. (b) ADI-HPML, CNDS-HPML, CNAFS-HPML and HIE-HPML CFLN = 3. (c) ADI-HPML, CNDS-HPML, CNAFS-HPML and HIE-HPML CFLN = 6.

Figure 7 and 8 show the RMS with different CFLNs and PML algorithms of RCP/LCP transmission and reflection coefficients.

Due to the FDTD-PML and FDTD-HPML is merely stable with CFLN = 1, they are not included here. It can be concluded both form Fig. 7 and Fig. 8 that the RMS error increases with the enlargement of CFLNs. That means the calculation accuracy decreases with the increment of CFLNs. The reason can also be concluded that the numerical

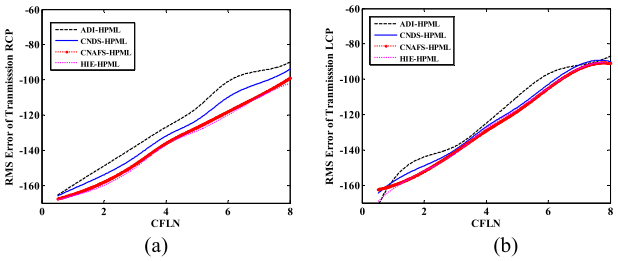

FIGURE 7. The RMS error (a) Transmission RCP wave. (b) Transmission RCP wave.

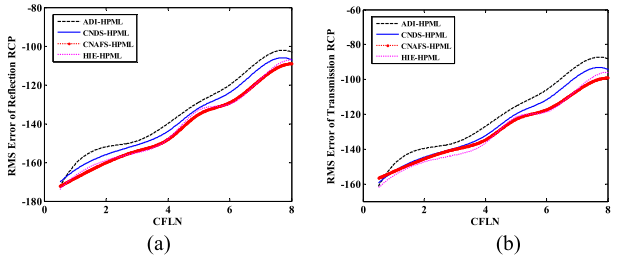

FIGURE 8. The RMS error (a) Reflection RCP wave. (b) Reflection RCP wave.

dispersion increases with the increment of CFLNs. Meanwhile, although the RMS error shows its maximum value with CFLN = 8, they still below −80 dB which is accuracy enough in the practical engineering.

Although all the PML algorithms hold considerable accuracy, the proposed HIE-HPML scheme can improve the accuracy compared with the published schemes. It can be concluded that the ADI-HPML holds the highest RMS error indicating it holds the worst performance. The CNDS-HPML shows better performance compared with ADI-HPML experimentally. The proposed procedure shows better accuracy compared with ADI-HPML and CNDS-HPML. In addition, it holds the similar performance with CNAFS-HPML. Thus, it can be concluded that the proposed scheme shows its better accuracy during the simulation. The effectiveness of the PML algorithms can not only be reflected by the calculation accuracy but also the efficiency and computational resources. Table 1 shows the CPU time, memory consumption, CFLN and time reduction obtained by different PML algorithms in the simulation of anisotropic gyrotropic plasma slab model. Through the Table 1, it can be concluded that compared with FDTD-PML, the computation becomes more expensive by introducing the higher order formulation. The reason is that more auxiliary variables and matrices should be solved during each iteration step. Meanwhile, the computational resources also become more expensive compared with the algorithms which are based on the conventional FDTD algorithm. The reason is that tri-diagonal matrices must be solved within the implicit algorithms. The employment of the Thomas algorithm results in the increment of both computational resources and running time. Within the implicit updating algorithms, the ADI and CNAFS procedure show the worst efficiency. Although the CNDS procedure can improve the efficiency during the whole simulation, six matrices still

TABLE 1. Computational time and occupied memory used by the different PML algorithms with different CFLNs of the anisotropic gyrotropic plasma slab model.

PML Algorithm	CFLN	Memory (G)	Time (m)	Time Reduction (%)
FDTD-PML	1	1.2	39.3	-
FDTD-HPML	1	1.6	55.1	-40.2
ADI-HPML	1	2.7	374.4	-852.7
CNDS-HPML	1	2.1	339.7	-764.4
CNAFS-HPML	1	2.9	363.0	-823.7
HIE-HPML	1	1.8	103.1	-162.3
ADI-HPML	3	2.7	171.8	-337.2
CNDS-HPML	3	2.1	150.1	-281.9
CNAFS-HPML	3	2.9	165.9	-322.1
HIE-HPML	3	1.8	40.7	-3.5
ADI-HPML	6	2.9	89.0	-126.5
CNDS-HPML	6	2.1	78.8	-100.5
CNAFS-HPML	6	2.9	86.1	-119.1
HIE-HPML	6	1.8	22.5	42.7

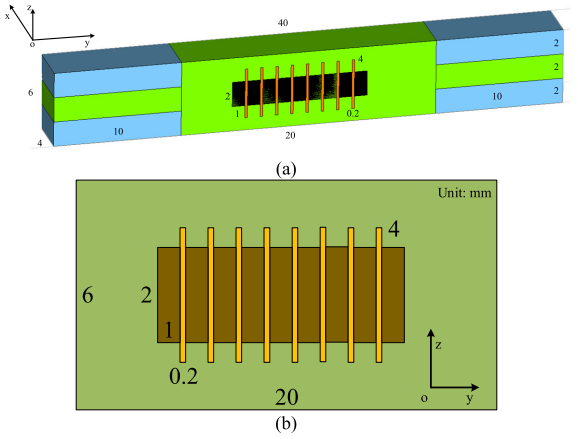

FIGURE 9. The sketch picture of waveguide structure (a) detail parameters. (b) Front view from yOz plane.

should be calculated at each time step. The proposed HIE procedure can improve the efficiency with lower CFLNs. Such phenomenon indicates the proposed scheme has significant advantage compared with published algorithms. In conclusion, the proposed procedure shows the higher accuracy which is the similar as CNAFS procedure and efficiency which is the best among these algorithms.

B. WAVE PROPAGATION PROBLEM: AN ANISOTROPIC GYROTROPIC PLASMA/DIELECTRIC WAVEGUIDE STRUCTURE

For considering much more complex and practical circumstance, a wave propagation problem is undertaken. The wave propagation problem is demonstrated through waveguide structure which is composed of anisotropic gyrotropic plasma and dielectric block. Physical size and detail parameters are shown in Fig. 9.

The entire structure can be regarded as the combination of three mediums including anisotropic gyrotropic plasma, dielectric bulk and vacuum. The entire structure can be divided into three parts along y-direction. At the left and right sides of y-direction, they are composed of three layers which include vacuum, gyrotropic plasma and vacuum with

the uniform dimensions of $10 \times 4 \times 2$ mm along vertical z-direction. The parameters of anisotropic gyrotropic plasma are $\omega_p = 2\pi \times 28.7$ GHz, $\omega_b = 0.1$ Trad/s and $\nu = 20$ GHz. In the middle of y-direction, the electric bulks with the dimensions of $1 \times 4 \times 2$ mm and $0.2 \times 4 \times 4$ mm and electric parameters of $\varepsilon_r = 2.9$ and $\varepsilon_r = 4.7$. The front view obtained by yOz plane of the waveguide structure is shown in Fig. 9(b). The bulks are located at the center of z-direction. Nine $\varepsilon_r = 2.9$ bulks and Eight $\varepsilon_r = 4.7$ bulks are located along y-direction. The centre of fourth $\varepsilon_r = 4.7$ bulk is located at the center of the entire structure. The rest part is filled with gyrotropic plasma. The plane wave incidents from the plasma regions at the left of the structure which is a modulated Gaussian pulse with the center frequency of 37.5 GHz and bandwidth of 12.5 GHz. The observation point which is used to evaluate the wave reflection occurred by PML regions is situated at the corner of the port. The observation port is located in the plasma region at the right side with the distance of one grid of PML regions. The boundaries of the x- and z-directions are terminated by the perfectly electronic conductor (PEC). The boundaries of y-direction are terminated by 10-cell-PML to absorb outgoing waves and reduce wave reflections. Through the try and error method, the parameters inside the PML regions are chosen to obtain the best performance both in the time domain and frequency domain. The parameters of higher order PML formulation based algorithms are $\kappa_{\eta 1} = 270$, $\alpha_{\eta 1} = 0.1$, $m_{\eta 1} = 2$, $\sigma_{\eta 1\_\max} = 0.9\sigma_{\eta 1\_opt}$, $\kappa_{\eta 2} = 1$, $\alpha_{\eta 2} = 1.7$, $m_{\eta 2} = 1$, $\sigma_{\eta 2\_\max} = 0.001\sigma_{\eta 2\_opt}$. The parameters of CFS-PML based PML algorithms are chosen as $\kappa_\eta = 240$, $\alpha_\eta = 2.1$, $m_\eta = 3$, $\sigma_{\eta\_\max} = 0.7\sigma_{\eta\_opt}$.

It can be concluded from Fig. 9 that the uniform size along x-direction lead to the complex mesh generation. The HIE procedure is one of the most efficient ways to alleviate such condition. The mesh sizes are chosen as $\Delta x = 0.05$ mm and $\Delta y = \Delta z = 0.1$ mm. The corresponding time step can be obtained as $\Delta t_{\max}^{FDTD} = 96.2$ fs. The performance of various PML algorithms can be reflected by the relative reflection error in the time domain which can be given as

$$R_{dB}(t) = 20\log_{10}\left[\left|E_z^t(t) - E_z^r(t)\right| / \left|\max\{E_z^r(t)\}\right|\right] \quad (15)$$

where $E_z^t(t)$ is the test solution which is obtained at the observation point directly, $E_z^r(t)$ is the reference solution which can be calculated by enlarging the domain by 20 times and terminating by 64-cell-PML. Figure 10 shows the waveform at the observation point with different PML algorithms and CFLNs. The CFL number (CFLN) can be defined as $CFLN = \Delta t / \Delta t_{\max}^{FDTD}$. Within the equation, Δt is the time step in the algorithms whose stability can break the CFL condition. As can be concluded from Fig. 10(a), the waveforms are almost overlapped with CFLN = 1. Such phenomenon indicates these algorithms almost hold the similar accuracy and performance with CFLN = 1. From Fig. 10(b) and 10(c), it can be observed that the accuracy decreases with the increment of CFLNs, due to the increment of numerical dispersion. In addition, it can be observed that the CNAFS-HPML and

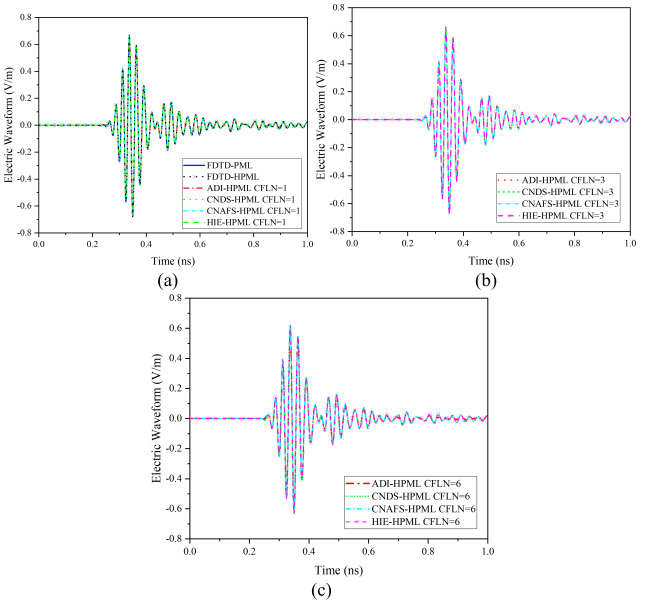

FIGURE 10. The waveform at the observation point (a) FDTD-PML, FDTD-HPML, ADI-HPML, CNDS-HPML, CNAFS-HPML and HIE-HPML CFLN = 1. (b) ADI-HPML, CNDS-HPML, CNAFS-HPML and HIE-HPML CFLN = 3. (c) ADI-HPML, CNDS-HPML, CNAFS-HPML and HIE-HPML CFLN = 6.

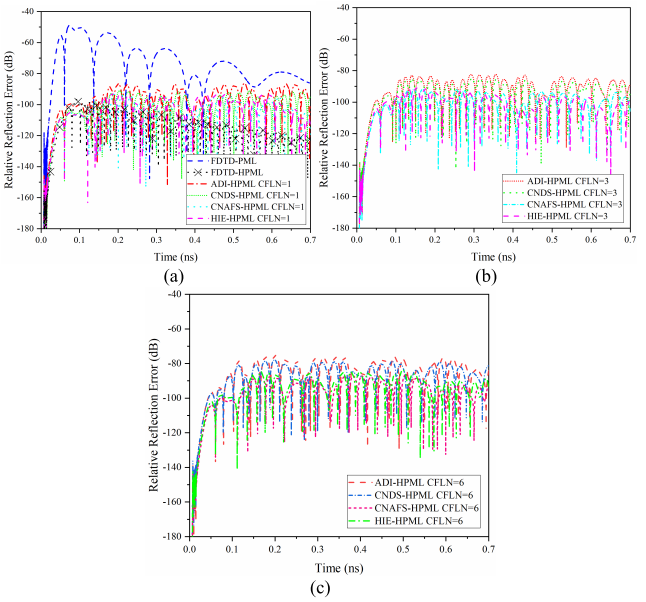

FIGURE 11. The relative reflection error in the time domain. (a) FDTD-PML, FDTD-HPML, ADI-HPML, CNDS-HPML, CNAFS-HPML and HIE-HPML CFLN = 1. (b) ADI-HPML, CNDS-HPML, CNAFS-HPML and HIE-HPML CFLN = 3. (c) ADI-HPML, CNDS-HPML, CNAFS-HPML and HIE-HPML CFLN = 6.

proposed HIE-HPML hold the similar accuracy and performance. The ADI-HPML has the worst performance among the implicit PML algorithms. Such phenomenon indicates that the ADI procedure has the largest numerical dispersion among them. It can be concluded that the proposed HIE-HPML can receive enhanced performance in the wave propagation problem.

The absorption performance of the PML, relative reflection error, in the time domain obtained by different PML

TABLE 2. Computational time and occupied memory used by the different PML algorithms with different CFLNs of the waveguide structure.

PML Algorithm	CFLN	Memory (GB)	Time (m)	Time Reduction (%)
FDTD-PML	1	1.7	42.7	-
FDTD-HPML	1	2.3	61.4	-43.8
ADI-HPML	1	3.1	411.0	-862.6
CNDS-HPML	1	2.9	358.1	-738.6
CNAFS-HPML	1	3.4	397.3	-830.4
HIE-HPML	1	2.5	119.9	-180.8
ADI-HPML	3	3.1	189.0	-342.6
CNDS-HPML	3	2.9	162.2	-279.9
CNAFS-HPML	3	3.4	177.4	-315.5
HIE-HPML	3	2.5	45.0	-5.4
ADI-HPML	6	3.1	94.3	-120.8
CNDS-HPML	6	2.9	80.8	-89.2
CNAFS-HPML	6	3.4	89.5	-109.6
HIE-HPML	6	2.5	24.1	43.6

algorithms and CFLN is shown in Fig. 11. It can be observed that the FDTD-HPML hold the best absorption not only in the maximum value but also in the late-time reflections. Meanwhile, compared with FDTD-PML, they can be further enhanced as well. Such condition indicates that the introduction of higher order PML formulation can improve the absorption during the simulation. As shown in Fig. 11(a) that compared with FDTD-PML, the other higher order based PML formulation can further enhance the performance during the whole simulation. Such phenomenon indicates the effectiveness of the higher order PML formulation. By observing Fig. 11 (b) and Fig. 11 (c), the entire performance decreases with the increment of CFLNs due to the enlargement of numerical dispersion. It can be concluded from the group of Fig. 11 that the CNAFS-HPML and HIE-HPML almost hold the same absorption. The FDTD-HPML and ADI-HPML is with the worst and best among the implicit algorithms, respectively. Most importantly, the HIE-HPML with CFLN $= 6$ hold the better performance compared with FDTD-PML. Such condition indicates that the proposed scheme has considerable effectiveness in absorption. Table 2 shows the memory consumption, CFLN, CPU time and time reduction of different PML algorithms. It can be observed that the introduction of higher order concept increases the running time and memory consumption. However, the increment of absorption indicates the effectiveness of the higher order formulation. Compared with the conventional FDTD based algorithms including FDTD-PML and FDTD-HPML, the implicit PML algorithms increases the memory and running time at lower CFLNs. The reason is that several matrices should be calculated at each time step. The running time can be shorten with the increment of CFLNs. The reason is that the larger CFLN can obtain larger time step resulting in the decrement of total iteration time steps. Especially, it should be noticed that the proposed scheme with CFLN $= 6$ can receive the best efficiency among these algorithms. Meanwhile, it can obtain considerable performance during the simulation.

The accuracy and performance of various PML algorithms can also be reflected by the Scattering-Parameters (S parameter) in the frequency domain alternatively including the

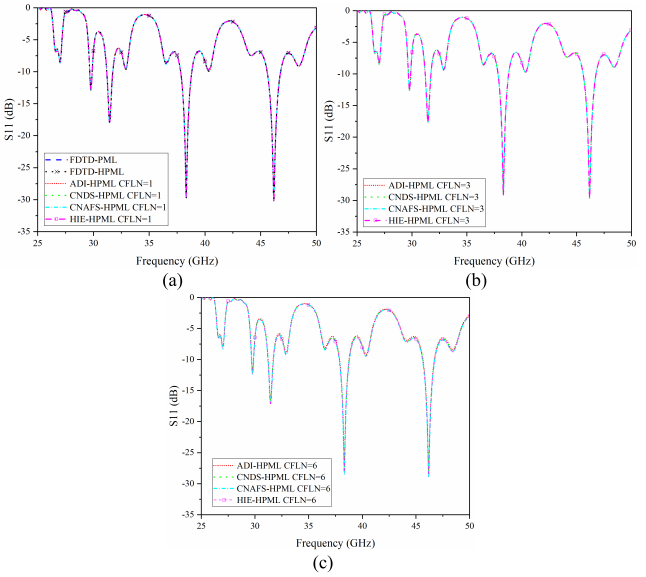

FIGURE 12. The return loss in the frequency domain. (a) FDTD-PML, FDTD-HPML, ADI-HPML, CNDS-HPML, CNAFS-HPML and HIE-HPML CFLN = 1. (b) ADI-HPML, CNDS-HPML, CNAFS-HPML and HIE-HPML CFLN = 3. (c) ADI-HPML, CNDS-HPML, CNAFS-HPML and HIE-HPML CFLN = 6.

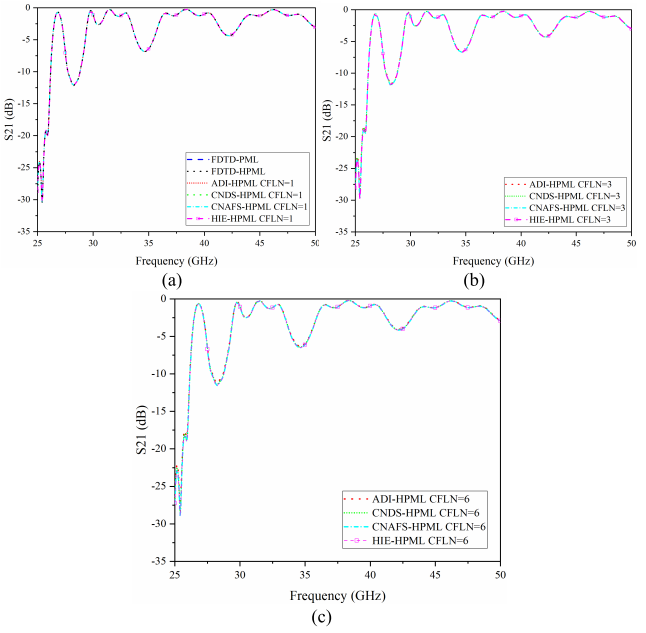

FIGURE 13. The transmission coefficient in the frequency domain. (a) FDTD-PML, FDTD-HPML, ADI-HPML, CNDS-HPML, CNAFS-HPML and HIE-HPML CFLN = 1. (b) ADI-HPML, CNDS-HPML, CNAFS-HPML and HIE-HPML CFLN = 3. (c) ADI-HPML, CNDS-HPML, CNAFS-HPML and HIE-HPML CFLN = 6.

return loss (S_{11}) and transmission coefficient (S_{21}) within the waveguide problem. Figure 12 and 13 show the S_{11} and S_{12} of the waveguide problem obtained by different PML algorithms and CFLNs. It can be concluded both from Fig. 12(a) and Fig. 13(a) that the S parameters are almost overlapped indicating all of the PML algorithms almost hold the calculation accuracy. From Fig. 12(b)-(c) and Fig. 13(b)-(c), it can be observed that the increment of CFLNs results in the

decrement of accuracy. Meanwhile, it can also be concluded that the CNAFS-HPML holds the similar accuracy with the proposed HIE-HPML.

From Fig. 13, the proposed HIE-HPML can receive better simulation accuracy which is the similar with CNAFS-HPML. Meanwhile, due to the calculation of two tri-diagonal matrices, the proposed scheme can significantly reduce the simulation duration compared with the unconditionally algorithms, for example, ADI-HPML, CNDS-HPML and CNAFS-HPML. In summary, the proposed scheme shows its suitable in gyrotropic plasma with fine geometry details along single direction.

IV. CONCLUSION

The HIE-HPML is proposed in the anisotropic gyrotropic plasma by incorporating the HIE procedure and higher order formulation. The anisotropic gyrotropic plasma is calculated through the bilinear transform method which can maintain considerable accuracy, stability and efficiency. Through the anisotropic gyrotropic plasma slab simulation, the effectiveness of the algorithm is demonstrated through the comparison with analytic resolution. The results indicate that the proposed scheme can not only receive considerable accuracy but also obtain better efficiency. Such conclusion can be further testified through the waveguide structure in the second numerical example. It also can be concluded that the proposed scheme can obtain better absorption. The proposed scheme takes full advantages of HIE procedure, higher order formulation and bilinear transform method in terms of efficiency, accuracy and absorption.

REFERENCES

[1] K. Abdijalilov and H. Grebel, "Z-transform theory and FDTD stability," *IEEE Trans. Antennas Propag.*, vol. 52, no. 11, pp. 2950–2954, Nov. 2004.

[2] K. Yee, "Numerical solution of initial boundary value problems involving Maxwell's equations in isotropic media," *IEEE Trans. Antennas Propag.*, vol. AP-14, no. 3, pp. 302–307, May 1966.

[3] M. Yan, K. R. Shao, X. W. Hu, Y. Guo, J. Zhu, and J. D. Lavers, "Z-transform-based FDTD analysis of perfectly conducting cylinder covered with unmagnetized plasma," *IEEE Trans. Magn.*, vol. 43, no. 6, pp. 2968–2970, Jun. 2007.

[4] J. M. Jin, *The Finite Element Method in Electromagnetics*, 3rd ed. New York, NY, USA: Wiley, 2014.

[5] A. Taflove and S. C. Hagness, *Computational Electrodynamics: The Finite-Difference Time-Domain Method*, 3rd ed. Boston, MA, USA: Artech House, 2005.

[6] T. Namiki, "3-D ADI-FDTD method-unconditionally stable time-domain algorithm for solving full vector Maxwell's equations," *IEEE Trans. Microw. Theory Techn.*, vol. 48, no. 10, pp. 1743–1748, 2000.

[7] J. Shibayama, M. Muraki, J. Yamauchi, and H. Nakano, "Efficient implicit FDTD algorithm based on locally one-dimensional scheme," *Electron. Lett.*, vol. 41, no. 19, pp. 1046–1047, Sep. 2005.

[8] G. Sun and C. W. Trueman, "Efficient implementations of the Crank-Nicolson scheme for the finite-difference time-domain method," *IEEE Trans. Microw. Theory Techn.*, vol. 54, no. 5, pp. 2275–2284, May 2006.

[9] J. Chen and J. Wang, "A three-dimensional semi-implicit FDTD scheme for calculation of shielding effectiveness of enclosure with thin slots," *IEEE Trans. Electromagn. Compat.*, vol. 49, no. 2, pp. 354–360, May 2007.

[10] J. Chen and J. Wang, "Numerical simulation using HIE-FDTD method to estimate various antennas with fine scale structures," *IEEE Trans. Antennas Propag.*, vol. 55, no. 12, pp. 3603–3612, Dec. 2007.

[11] J. Chen and J. Wang, "Three-dimensional dispersive hybrid implicit–explicit finite-difference time-domain method for simulations of graphene," *Comput. Phys. Commun.*, vol. 207, pp. 211–216, Oct. 2016.

[12] K. Niu, Z. Huang, X. Ren, M. Li, B. Wu, and X. Wu, "An optimized 3-D HIE-FDTD method with reduced numerical dispersion," *IEEE Trans. Antennas Propag.*, vol. 66, no. 11, pp. 6435–6440, Nov. 2018.

[13] K. Niu, Z. Huang, X. Ren, K. Xu, M. Li, X. Wu, P. Li, L. Jiang, and H. Bagci, "An efficient 3-D stochastic HIE-FDTD algorithm for investigation of statistical variation in electromagnetic field," *IEEE Trans. Antennas Propag.*, vol. 68, no. 12, pp. 8227–8232, Dec. 2020.

[14] Z. Liu, Y. Chen, X. Sun, and Y. Liu, "Implementation of CFS-PML for HIE-FDTD method," *IEEE Antennas Wireless Propag. Lett.*, vol. 11, pp. 381–384, 2012.

[15] F. Xiao, X. Tang, and L. Wang, "Stability and numerical dispersion analysis of a 3D hybrid implicit-explicit FDTD method," *IEEE Trans. Antennas Propag.*, vol. 56, no. 10, pp. 3346–3350, Oct. 2008.

[16] Y.-D. Kong, C.-B. Zhang, and Q.-X. Chu, "An optimized one-step leapfrog HIE-FDTD method with the artificial anisotropy parameters," *IEEE Trans. Antennas Propag.*, vol. 68, no. 2, pp. 1198–1203, Feb. 2020.

[17] J.-P. Berenger, "A perfectly matched layer for the absorption of electromagnetic waves," *J. Comput. Phys.*, vol. 114, no. 2, pp. 185–200, Oct. 1994.

[18] J. P. Berenger, *Perfectly Matched Layer (PML) for Computational Electromagnetics*. San Mateo, CA, USA: Morgan, 2007.

[19] W. C. Chew and W. H. Weedon, "A 3D perfectly matched medium from modified Maxwell's equations with stretched coordinates," *Microw. Opt. Technol. Lett.*, vol. 7, no. 13, pp. 599–604, Sep. 1994.

[20] M. Kuzuoglu and R. Mittra, "Frequency dependence of the constitutive parameters of causal perfectly matched anisotropic absorbers," *IEEE Microw. Guided Wave Lett.*, vol. 6, no. 12, pp. 447–449, Dec. 1996.

[21] D. Correia and J.-M. Jin, "On the development of a higher-order PML," *IEEE Trans. Antennas Propag.*, vol. 53, no. 12, pp. 4157–4163, Dec. 2005.

[22] D. Correia and J.-M. Jin, "Performance of regular PML, CFS-PML, and second-order PML for waveguide problems," *Microw. Opt. Technol. Lett.*, vol. 48, no. 10, pp. 2121–2126, 2006.

[23] N. Feng, Y. Yue, C. Zhu, L. Wan, and Q. H. Liu, "Second-order PML: Optimal choice of nth-order PML for truncating FDTD domains," *J. Comput. Phys.*, vol. 285, pp. 71–83, Mar. 2015.

[24] Z. Xu, X. Ma, Q. Liu, and Z. Bai, "Bilinear transform implementation of the higher-order PML," in *Proc. 6th Int. Conf. Electromagn. Field Problems Appl.*, Jun. 2012, pp. 1–4.

[25] X.-K. Wei, W. Shao, S.-B. Shi, Y.-F. Cheng, and B.-Z. Wang, "An optimized higher order PML in domain decomposition WLP-FDTD method for time reversal analysis," *IEEE Trans. Antennas Propag.*, vol. 64, no. 10, pp. 4374–4383, Oct. 2016.

[26] X.-K. Wei, W. Shao, H. Ou, and B.-Z. Wang, "Efficient WLP-FDTD with complex frequency-shifted PML for super-resolution analysis," *IEEE Antennas Wireless Propag. Lett.*, vol. 16, pp. 1007–1010, 2017.

[27] J. Li, P. Wu, and H. Jiang, "Implementation of higher order CNAD CFS-PML for truncating unmagnetised plasma," *IET Microw., Antennas Propag.*, vol. 13, no. 6, pp. 756–760, May 2019.

[28] J. Li and P. Wu, "Unconditionally stable higher order CNAD-PML for left-handed materials," *IEEE Trans. Antennas Propag.*, vol. 67, no. 11, pp. 7156–7161, Nov. 2019.

[29] J. Li and C. Miao, "An efficient FDTD implementation of the CFS-PML based on the ADE method and its validation along with the PLRC method in dispersive media," in *Proc. Int. Conf. Microw. Millim. Wave Technol.*, Apr. 2008, pp. 766–769.

[30] T. Kashiwa, N. Yoshida, and I. Fukai, "Transient analysis of a magnetized plasma in three-dimensional space," *IEEE Trans. Antennas Propag.*, vol. AP-36, no. 8, pp. 1096–1105, Aug. 1988.

[31] N. Sternberg and J. Poggie, "Plasma-sheath transition in the magnetized plasma-wall problem for collisionless ions," *IEEE Trans. Plasma Sci.*, vol. 32, no. 6, pp. 2217–2226, Dec. 2004.

[32] B. T. Nguyen, C. Furse, and J. J. Simpson, "A 3-D stochastic FDTD model of electromagnetic wave propagation in magnetized ionosphere plasma," *IEEE Trans. Antennas Propag.*, vol. 63, no. 1, pp. 304–313, Jan. 2015.

[33] Y. Yu, J. Niu, and J. J. Simpson, "A 3-D global Earth-ionosphere FDTD model including an anisotropic magnetized plasma ionosphere," *IEEE Trans. Antennas Propag.*, vol. 60, no. 7, pp. 3246–3256, Jul. 2012.

[34] J. Wang, D. Zhang, C. Liu, Y. Li, Y. Wang, H. Qiao, and X. Li, "UNIPIC code for simulations of high power microwave devices," *Phys. Plasmas*, vol. 16, no. 3, Mar. 2009, Art. no. 033108.

[35] Y. Wang, J. Wang, Z. Chen, G. Cheng, and P. Wang, "Three-dimensional simple conformal symplectic particle-in-cell methods for simulations of high power microwave devices," *Comput. Phys. Commun.*, vol. 205, pp. 1–12, Aug. 2016.
[36] J. Liu, Z. Yan, J. Ji, Q. Chang, and H. Song, "Study on tunable magnetized plasma frequency selective surface using JEC-FDTD method," *IEEE Trans. Plasma Sci.*, vol. 48, no. 10, pp. 3479–3486, Oct. 2020.
[37] A. A. Al-Jabr, M. A. Alsunaidi, T. Ng, and B. S. Ooi, "A simple FDTD algorithm for simulating EM-wave propagation in general dispersive anisotropic material," *IEEE Trans. Antennas Propag.*, vol. 61, no. 3, pp. 1321–1326, Mar. 2013.
[38] Y. Yu and J. J. Simpson, "An E-J collocated 3-D FDTD model of electromagnetic wave propagation in magnetized cold plasma," *IEEE Trans. Antennas Propag.*, vol. 58, no. 2, pp. 469–478, Feb. 2010.
[39] S. Liu, J. Mo, and N. Yuan, "Piecewise linear current density recursive convolution FDTD implementation for anisotropic magnetized plasmas," *IEEE Microw. Wireless Compon. Lett.*, vol. 14, no. 5, pp. 222–224, May 2004.
[40] X.-Y. Huang, C.-M. Tong, and L.-X. Ma, "Improved $(FD)^2TD$ formulations based on Z transform for anisotropic plasma," in *Proc. IEEE Int. Conf. Prog. Informat. Comput.*, Dec. 2010, pp. 1170–1173.
[41] J.-S. Zhang, X.-L. Xi, Z.-W. Li, J.-F. Liu, and Y.-R. Pu, "An unconditionally stable WLP-FDTD model of wave propagation in magnetized plasma," *IEEE Trans. Plasma Sci.*, vol. 44, no. 1, pp. 25–30, Jan. 2016.
[42] J.-X. Liu, L. Ju, P. Du, Y.-J. Liu, and H.-W. Yang, "An improved cascaded SO-FDTD method for high temperature magnetized plasma," *Comput. Phys. Commun.*, vol. 235, pp. 153–158, Feb. 2019.
[43] P. Wu, Y. Xie, H. Jiang, and T. Natsuki, "Computationally efficient implicit ADI theory and its open region problems for anisotropic gyrotropic plasma simulations," *Adv. Theory Simul.*, vol. 3, no. 11, Nov. 2020, Art. no. 2000166.
[44] P. Wu, Y. Xie, H. Jiang, L. Niu, and T. Natsuki, "Computationally efficient complex envelope approximate Crank–Nicolson scheme and its open region problem for anisotropic gyrotropic plasma," *Phys. Plasmas*, vol. 27, no. 10, Oct. 2020, Art. no. 103302.
[45] J. Li and P. Wu, "Efficient PML implementation based on the unconditionally stable CN-FDTD algorithm for anisotropic magnetized plasma," *Optik*, vol. 171, pp. 468–475, Oct. 2018.
[46] K. Hosseini and Z. Atlasbaf, "Unconditionally stable LOD-FDTD method in anisotropic magnetized plasma," *IEEE Microw. Wireless Compon. Lett.*, vol. 27, no. 3, pp. 212–214, Mar. 2017.
[47] W. Song and H. Zhang, "Memory-optimized shift operator alternating direction implicit finite difference time domain method for plasma," *J. Comput. Phys.*, vol. 349, pp. 122–136, Nov. 2017.
[48] J. Cho, M.-S. Park, and K.-Y. Jung, "Perfectly matched layer for accurate FDTD for anisotropic magnetized plasma," *J. Electromagn. Eng. Sci.*, vol. 20, no. 4, pp. 277–284, Oct. 2020.
[49] P. Wu, Y. Xie, H. Jiang, and T. Natsuki, "Performance enhanced Crank-Nicolson boundary conditions for EM problems," *IEEE Trans. Antennas Propag.*, vol. 69, no. 3, pp. 1513–1527, Mar. 2021.

PEIYU WU (Graduate Student Member, IEEE) was born in Liaoning, China, in 1994. He received the B.Sc. and M.Sc. degrees from the School of Electronics and Information Engineering, Tianjin Polytechnic University, in 2016 and 2019, respectively. He is currently pursuing the Ph.D. degree with the School of Electronic and Information Engineering, Beihang University, Beijing.

His current research interests include computational electromagnetics, especially the FDTD algorithm and its unconditionally stable scheme, antenna design, microwave components, and electronic counter-measures.

HAN YU was born in 1985. He received the Ph.D. degree from the School of Astronautics, Harbin Institute of Technology, Harbin, China, in 2015.

He is currently a Senior Engineer with the Beijing Institute of Aerospace Systems Engineering, Beijing, China. His current research interests include parallel computing and nonlinear filters.

YONGJUN XIE received the B.Sc., M.Sc., and Ph.D. degrees in electronic engineering from Xidian University, Xian, China, in 1990, 1993, and 1996, respectively.

From March 1998 to November 1999, he joined The University of Texas at Dallas, Dallas, TX, USA, as a Postdoctoral Research Associate. From December 1999 to October 2001, he was a Postdoctoral Research Associate with Duke University. In October 2001, he joined Xidian University, as a Professor. In 2004, he was supported by the Program for the New Century Excellent Talents launched by Ministry of Education, China. Since 2009, he has been a Professor with Beihang University, Beijing, China. His research interests include computational electromagnetics, electromagnetic theory, microwave technology, antenna theory, microwave components, terahertz technology, and mobile telecommunication.

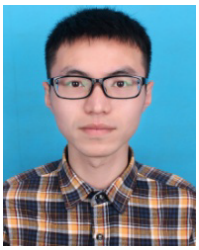

HAOLIN JIANG (Member, IEEE) was born in Chongqing, China, in 1989. He received the B.Sc. degree from the School of Electronic Engineering, Tianjin University of Technology and Education, in 2012, and the M.Sc. degree from the School of Electronics and Information Engineering, Tianjin Polytechnic University, in 2016. He is currently pursuing the Ph.D. degree with the School of Information Science and Engineering, Southeast University, Nanjing.

His current research interests include computational electromagnetics, especially the FDTD algorithm and its unconditionally stable scheme and parallel computing.

TOSHIAKI NATSUKI received the B.E. degree from the Beijing University of Chemical Technology, in 1984, and the Ph.D. degree from the Kyoto Institute of Technology, Japan, in 1994.

From 1995 to 1999, he was a Researcher with Hitachi Chemical Company Ltd., Japan. From 2000 to 2003, he worked for National Institute of Advanced Industrial Science and Technology, Japan. He is currently a Professor with the Faculty of Textile Science and Technology, Shinshu University, Japan. He has published more than 100 journal articles and many conference papers on his research fields and related topics. His current research interests include the design, fabrication, the structural analysis and evaluation of nano-materials, devices. He is currently an editorial board member of three international journals.